Electronic structure calculations results from LDA+U method

Vladimir I. Anisimov

Institute of Metal Physics
Ekaterinburg, Russia

LDA+U method applications

- **Mott insulators**
- **Polarons and stripes in cuprates**
- **Charge order: Fe_3O_4**
- **Spin order: calculation of exchange interaction parameters in CaV_nO_{2n+1}**
- **Orbital order: $KCuF_3$, $LaMnO_3$**
- **Charge and orbital order: $Pr_{0.5}Ca_{0.5}MnO_3$**
- **Low-spin to high-spin transition: Co^{+3} in $LaCoO_3$**
- **Magnetic transition in $FeSi_{1-x}Ge_x$ and vacancy magnetism in TiO_{2-x}**

LDA+U method applications

Mott insulators that are small gap semiconductors
or even metals in LSDA are correctly reproduced in LDA+U
as wide gap magnetic insulators with well localized d-electrons

Table 1. Experimental (exp) and calculated (LDA + U and LSDA) spin moment (m in μ_B) and energy gap (E in eV) values of the late-3d-transition-metal oxides.

	E_{LSDA}	E_{LDA+U}	E_{exp}	m_{LSDA}	m_{LDA+U}	m_{exp}
$CaCuO_2$	0.0	2.10	1.5	0.0	0.66	0.51
CuO	0.0	1.9	1.4	0.0	0.74	0.65
NiO	0.2	3.1	4.3, 4.0	1.0	1.59	1.77, 1.64, 1.90
CoO	0.0	3.2	2.4	2.3	2.63	3.35, 3.8
FeO	0.0	3.2	2.4	3.4	3.62	3.32
MnO	0.8	3.5	3.6–3.8	4.61	1.67	4.79, 4.58

V.Anisimov et al, Phys.Rev. B 44, 943 (1991)

LDA+U method applications

The density of states for ferromagnetic Gd metal from LDA+*U* calculation and results of BIS (bremsstrahlung isochromat spectroscopy) and XPS (x-ray photoemission spectroscopy) experiments.

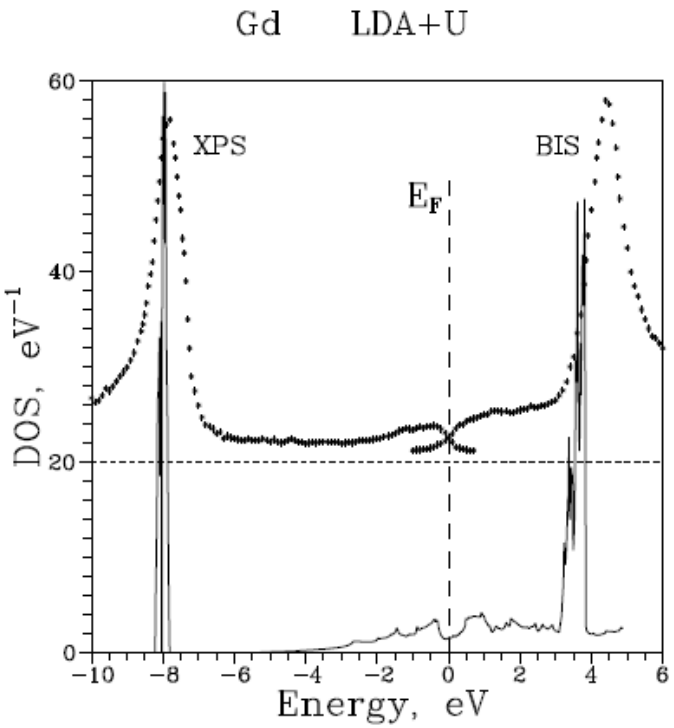

Antiferromagnetic Mott insulator $CaCuO_2$ (in LDA nonmagnetic metal)

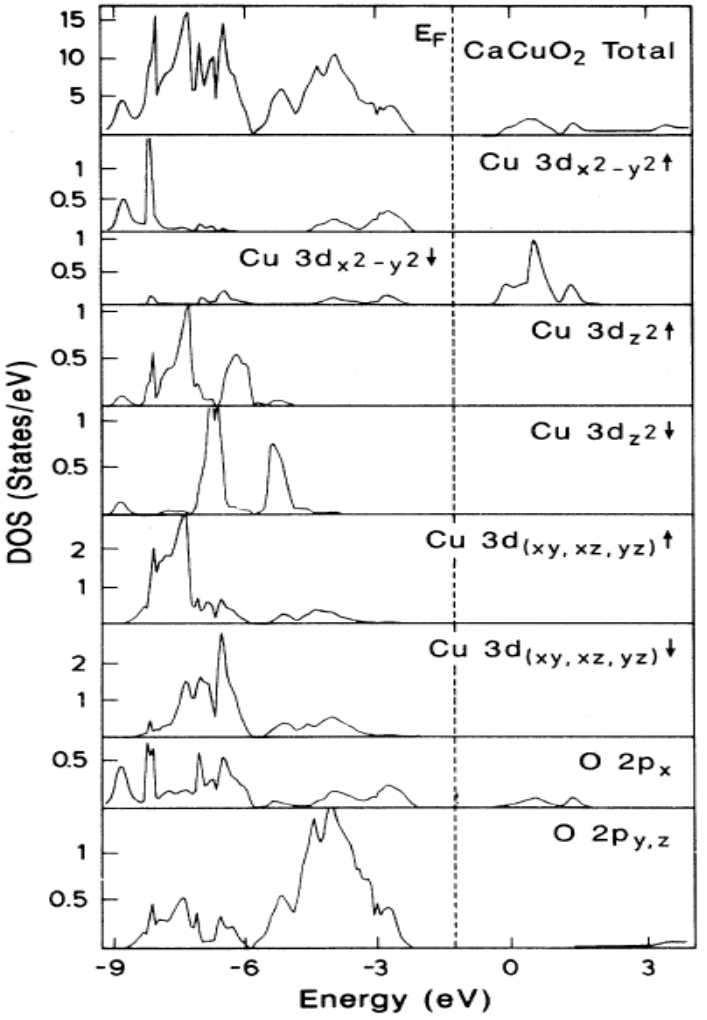

Polaron formation in cuprates and nickelates

A hole localization by local disruption of magnetic ordering (spin bag) and by lattice distortion in Mott insulators

TABLE I. The dependence of the total energy (δE, in meV) and the magnetic moments (μ, in μ_B) on the displacement (u) of either in-plane ("breathing," BR) or apical oxygens ("Jahn-Teller", JT) towards the central transition-metal ion (TM_1) in the supercell (TM_2 is the nearest and TM_3 the next-nearest TM_1 neighbor) in the case of "doped" La_2CuO_4 (LCO) and La_2NiO_4 (LNO).

	u	δE	μ_{TM_1}	μ_{TM_2}	μ_{TM_3}
LCO	0%	0	−0.55	−0.59	0.72
	2% (BR)	−39	−0.43	−0.63	0.73
	11% (JT)	15	0.96	−0.64	0.73
LNO	0%	0	0.42	−1.58	1.67
	4% (BR)	−210	0.54	−1.58	1.67

V.Anisimov et al, Phys.Rev.Lett. 68, 345 (1992)

Zhang-Rice singlet in $La_2Cu_{0.5}Li_{0.5}O_4$

Non-magnetic S=0 Cu^{+3} ion in CuO_4 clusters isolated by Li ions from each other

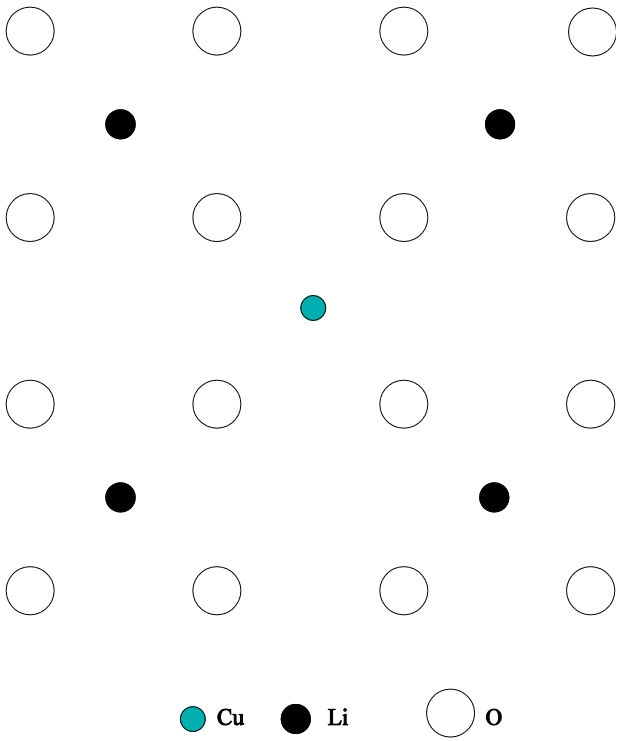

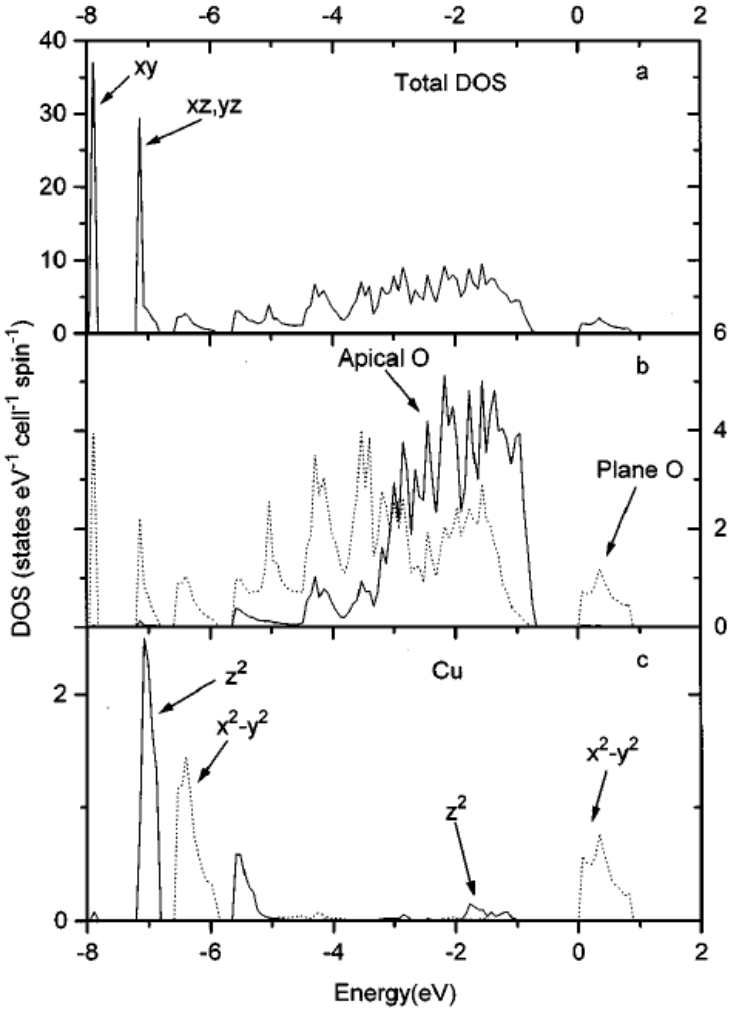

V.Anisimov et al, Phys.Rev.B 55, 12829 (1997)

t-J model parameters for distorted La_2CuO_4

Low-temperature tetragonal crystal structure of La_2CuO_4 can be presented as distorted (tilting and rotation of CuO_6 octahedra) high-temperature structure

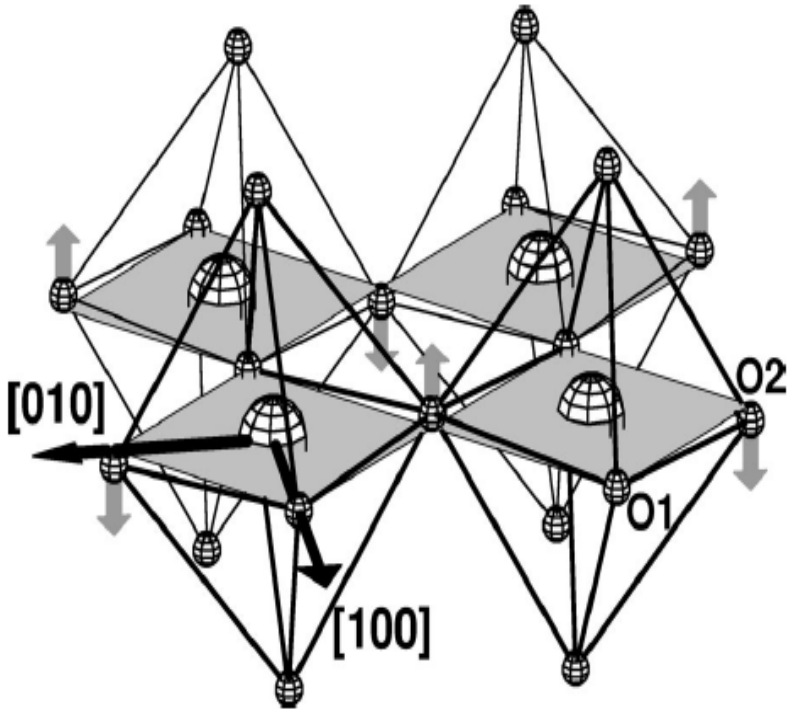

	Anisotropic		Isotropic	
τ	J_μ	t_μ	J_μ	t_μ
(1,0)	0.105	0.425	0.109	0.486
(0,1)	0.111	0.466	0.109	0.486
(1,1)	0.016	−0.064	0.016	−0.086
(2,0)	0	−0.001	0	−0.006
(0,2)	0	0.046	0	−0.006
(2,1)	0	0.014	0	0
(1,2)	0	0.036	0	0

V.Anisimov et al, Phys.Rev.B 66, 100502 (2002)

Stripe phase in cuprates ($La_{7/8}Sr_{1/8}CuO_4$)

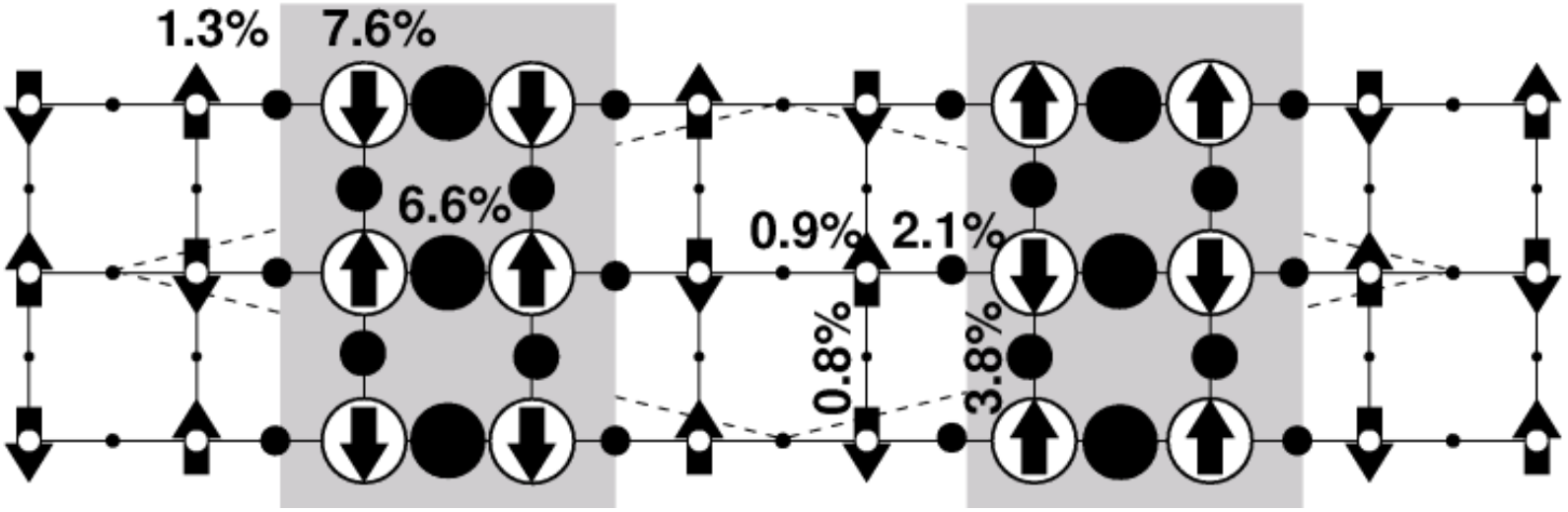

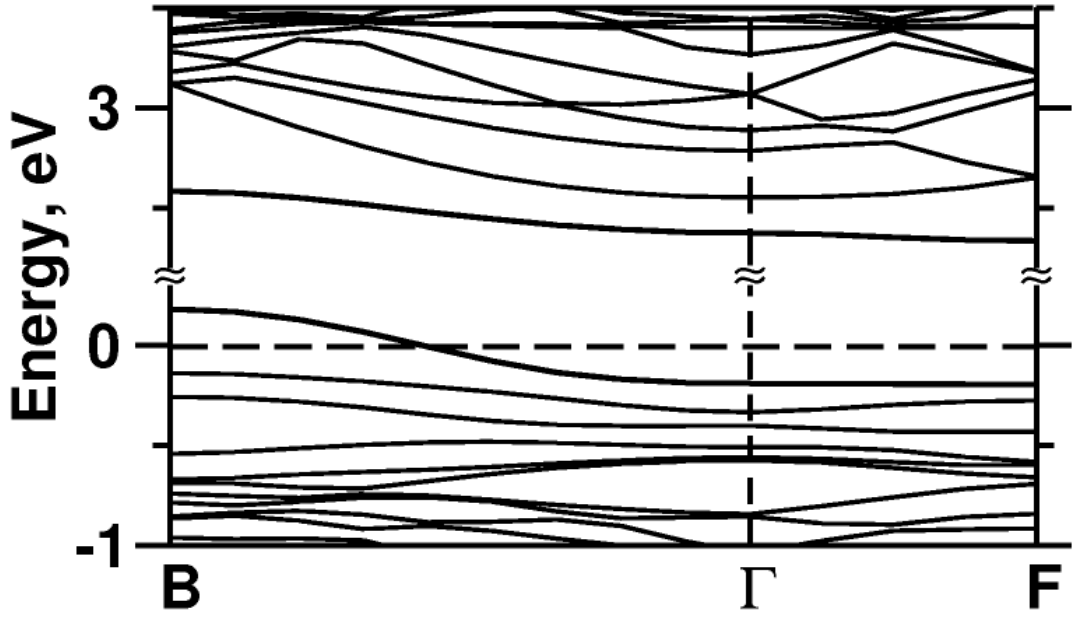

V.Anisimov et al, Phys. Rev. B 70, 172501 (2004)

Stripe phase in cuprates ($La_{7/8}Sr_{1/8}CuO_4$)

Angle resolved photoemission spectral weight integrated within 500 meV of the Fermi level, as a function of *kx* and *ky* together with calculated Fermi surface for 2D CuO_2 plane with stripes oriented along *y* (dashed line).

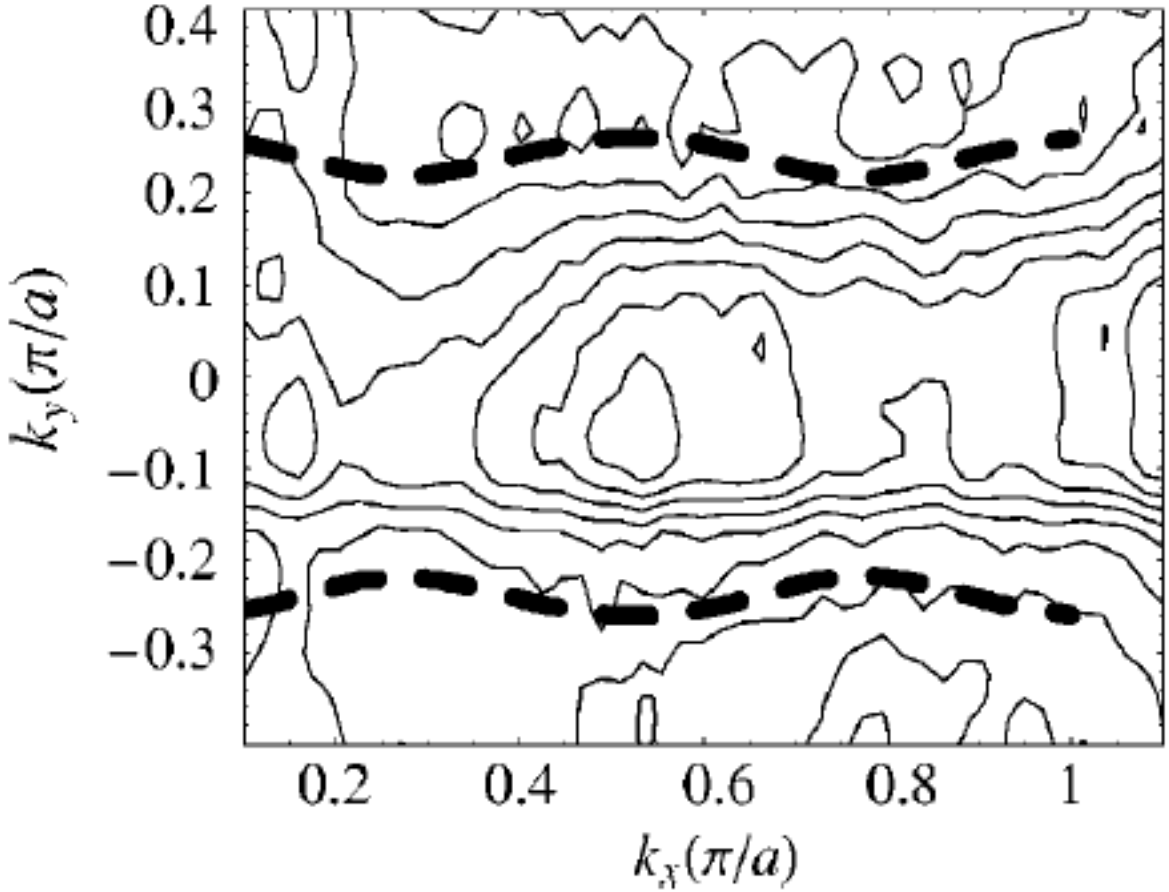

Wannier function for metallic stripe band

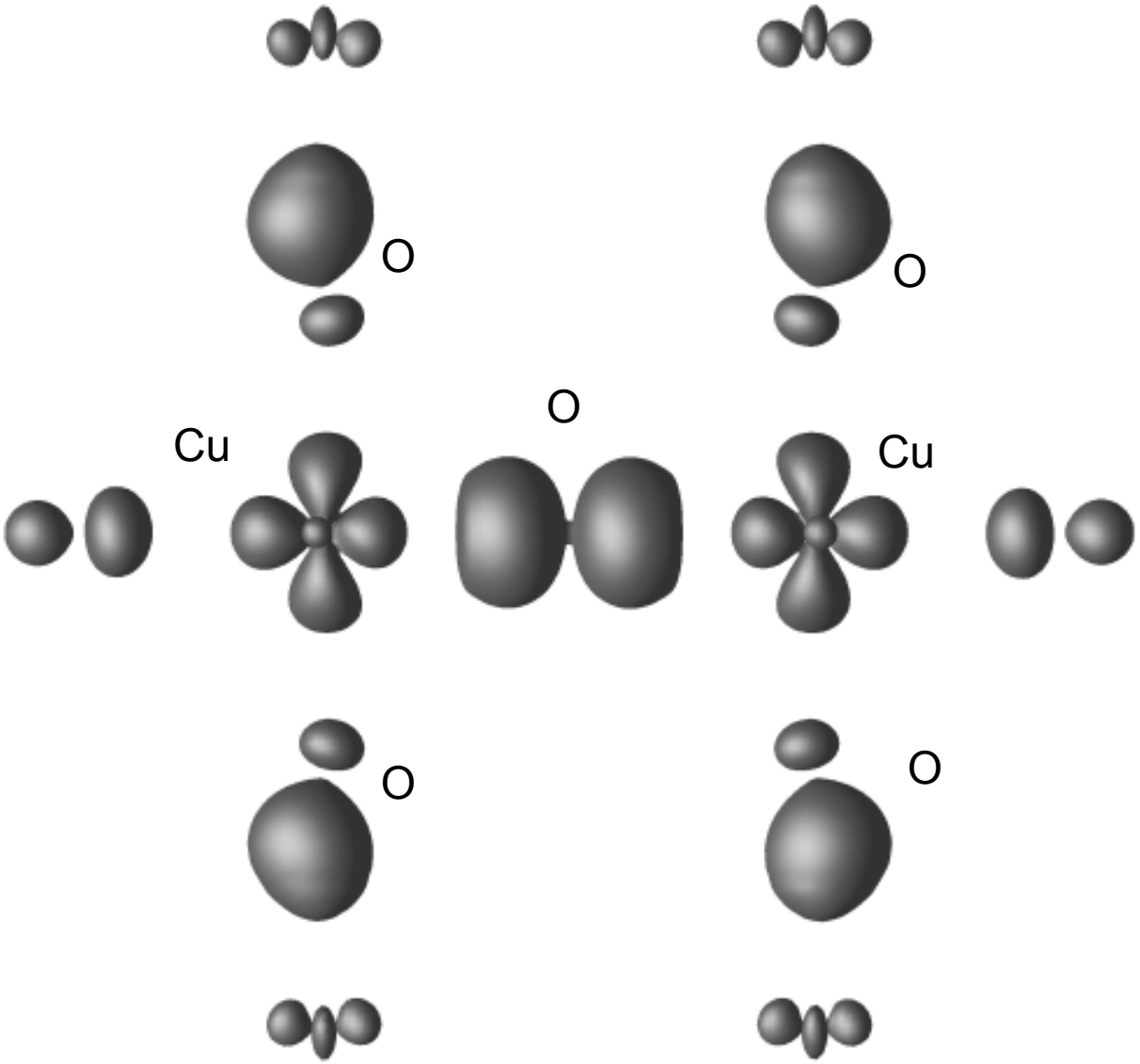

Exchange couplings for AF domain

Two-leg ladder

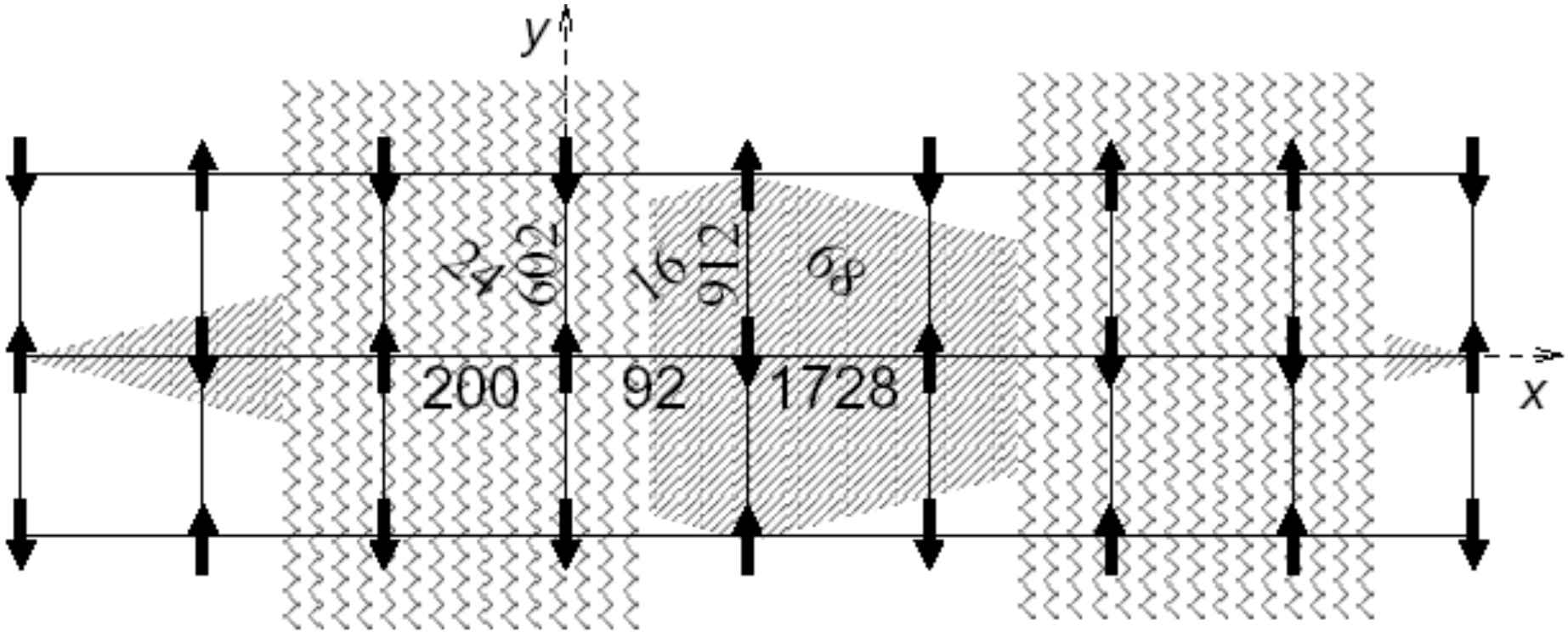

Charge order in Fe_3O_4

Fe_3O_4 has spinel crystal structure

one Fe^{+3} ion in tetrahedral position (A)

two $Fe^{+2.5}$ ions in octahedral positions (B)

Below T_V=122K a charge ordering happens ← **Verwey transition**

Simultaneous metal-insulator transition:

half of the octahedral positions is occupied by Fe^{+3} and other half by Fe^{+2}.

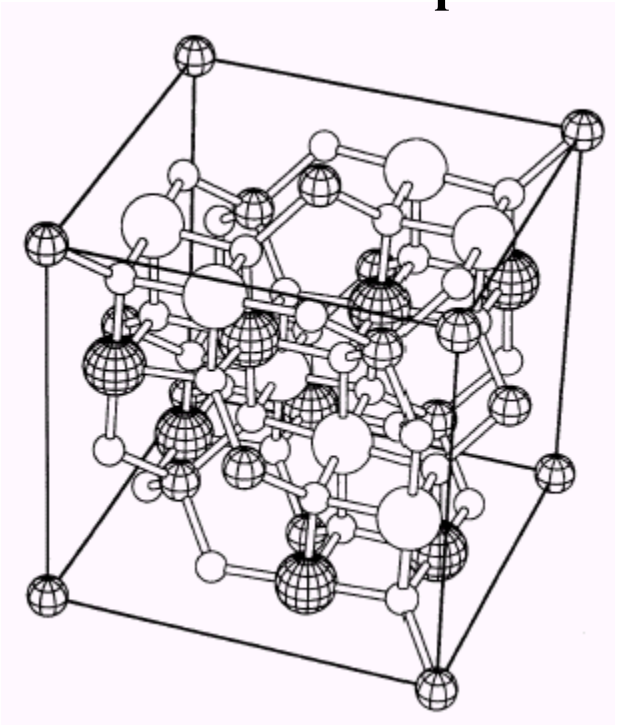

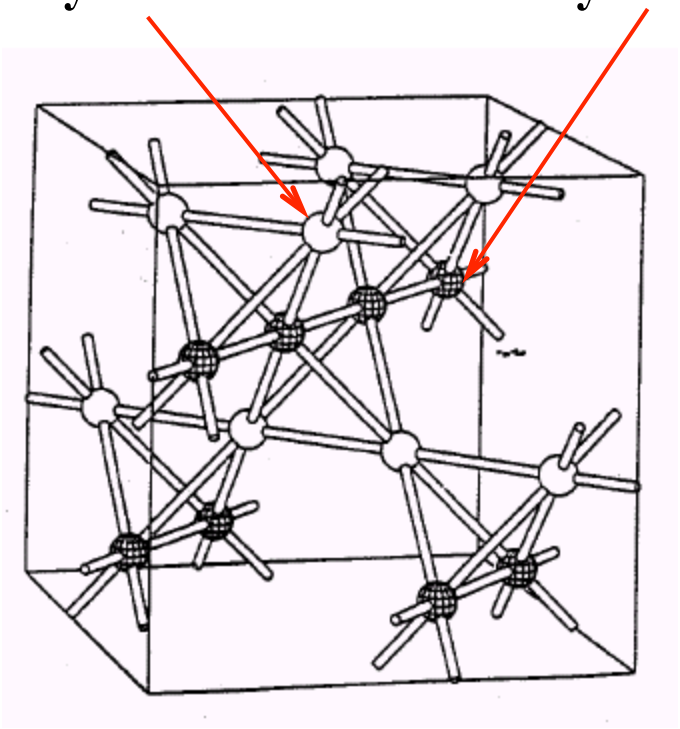

V.Anisimov et al, Phys. Rev.B 54, 4387 (1996)

LDA and charge order problem

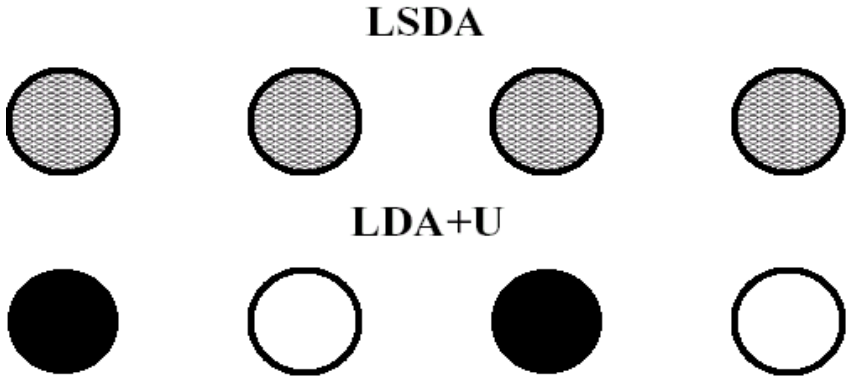

Charge disproportionation in LSDA is unstable due to self-interaction problem

$$U = \frac{d\varepsilon}{dn}; \qquad \varepsilon_1^{LSDA}(n_0 - \delta n) = \varepsilon_0 - U\delta n; \quad \varepsilon_2^{LSDA}(n_0 + \delta n) = \varepsilon_0 + U\delta n;$$

in LDA+U self-interaction is explicitly canceled

$$\varepsilon_1 = \varepsilon_1^{LSDA}(n_0 - \delta n) + U(\frac{1}{2} - (n_0 - \delta n)) = \varepsilon_0 - U(\frac{1}{2} - n_0)$$

$$\varepsilon_2 = \varepsilon_2^{LSDA}(n_0 + \delta n) + U(\frac{1}{2} - (n_0 + \delta n)) = \varepsilon_0 - U(\frac{1}{2} - n_0)$$

LSDA and LDA+U results for Fe_3O_4

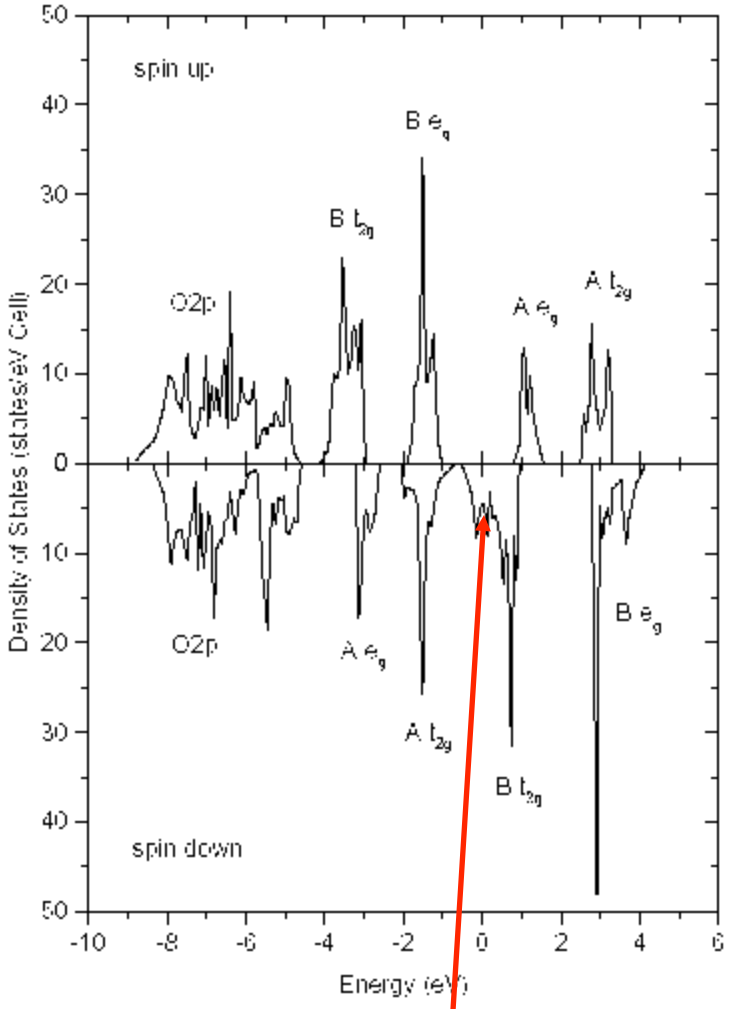

metal

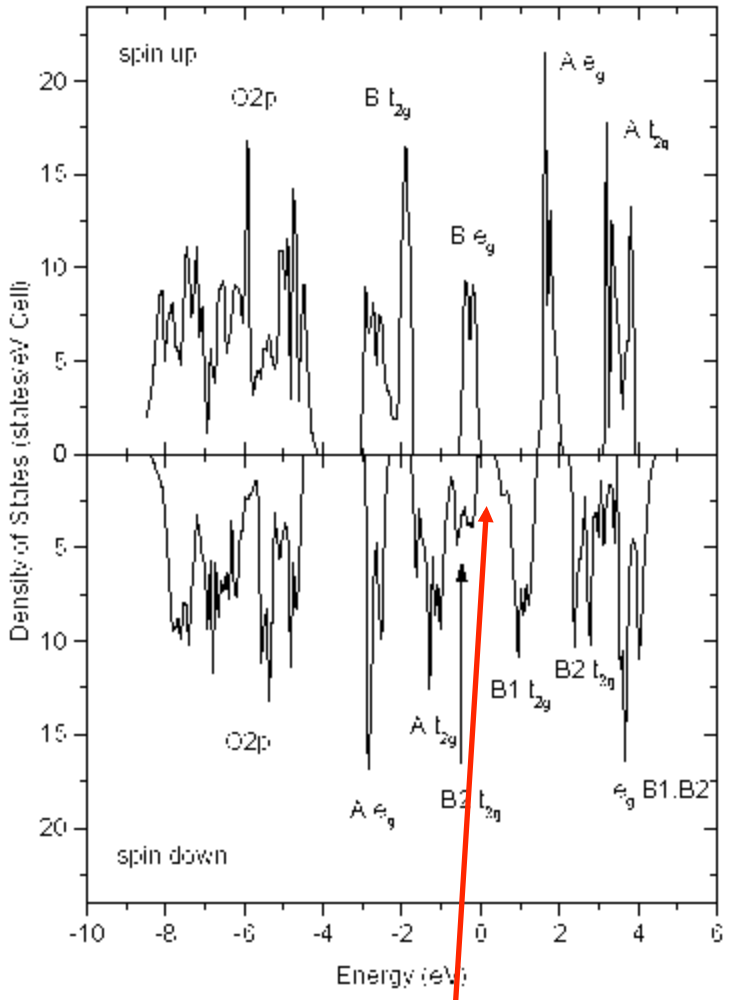

insulator

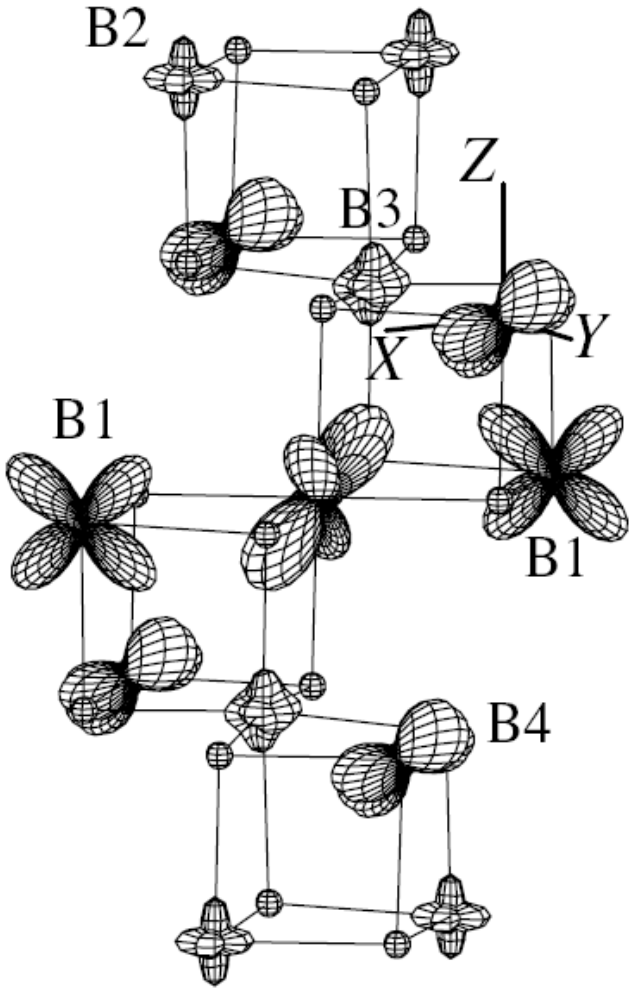

Charge and orbital order in experimental low-temperature monoclinic crystal structure Fe_3O_4

I.Leonov et al,
PRL93,146404 (2004)

Charge and orbital order in experimental low-temperature monoclinic crystal structure Fe_3O_4

TABLE I. Total and l-projected charges, magnetic moments, and occupation of the most populated t_{2g} minority orbitals calculated for inequivalent Fe_B ions in the low-temperature $P2/c$ phase of Fe_3O_4 [28].

Fe_B ion	q	q_s	q_p	q_d	M (μ_B)	$t_{2g\downarrow}$ orbital	n
Fe_{B1}	6.04	0.17	0.19	5.69	3.50	$d_{xz} \mp d_{yz}$	0.76
Fe_{B2}	5.73	0.19	0.21	5.44	3.94		0.09
Fe_{B3}	5.91	0.19	0.21	5.51	3.81		0.09
Fe_{B4}	6.03	0.16	0.18	5.69	3.48	$d_{x^2-y^2}$	0.80

Exchange interactions in layered vanadates

CaV_nO_{2n+1} (n=2,3,4) systems show a large variety of magnetic properties:

- **n=3: CaV_3O_7 has unusual long-range spin order**
- **n=4: CaV_4O_9 is a frustrated (plaquets) system with a spin gap value 107K**
- **n=2: CaV_2O_5 is a set of weakly coupled dimers with a large spin gap 616 K**
- **isostructural MgV_2O_5 has very small spin gap value < 10K**

Fully ab-initio description of magnetic properties

LDA+U calculations: eigenfunctions and eigenvalues → Exchange couplings calculations using LDA+U results → Heisenberg model is solved by QMC

V.Anisimov et al, Phys.Rev.Lett. 83, 1387 (1999)

Crystal structure of CaV_nO_{2n+1}

is formed by VO_5 pyramids connected into layers.

V^{+4} ions in d^1 configuration.

The occupied d_{xy}-orbital of V^{+4} ions in CaV_3O_7

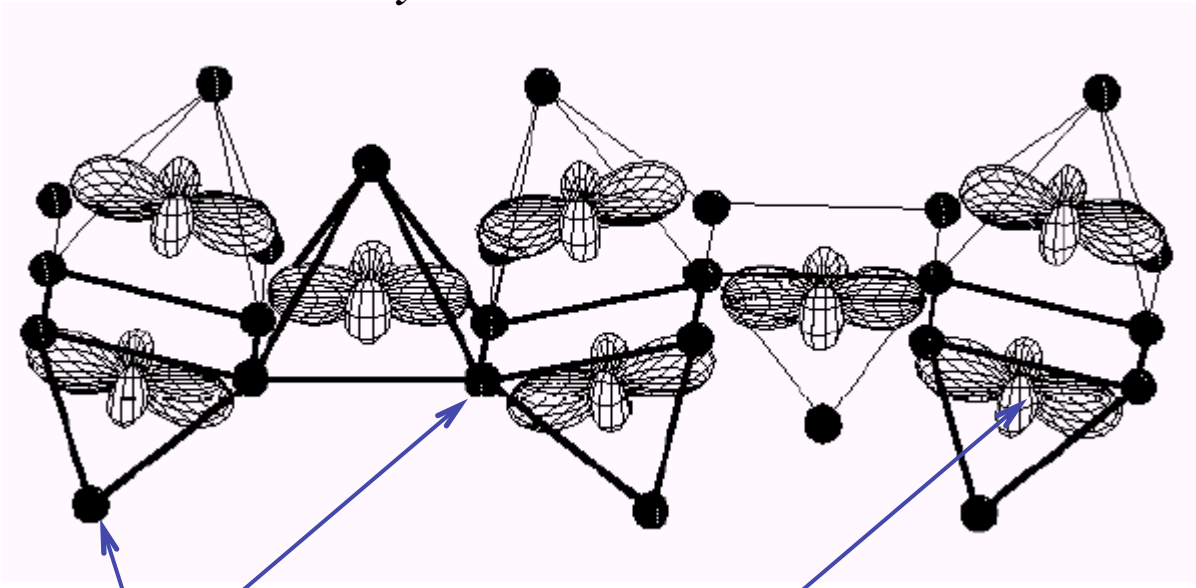

Oxygen atoms form pyramids with V atoms inside them.

Exchange couplings scheme

The basic crystal structure and the notation of exchange couplings in

CaV_2O_5 and MgV_2O_5 **CaV_3O_7** **CaV_4O_9**

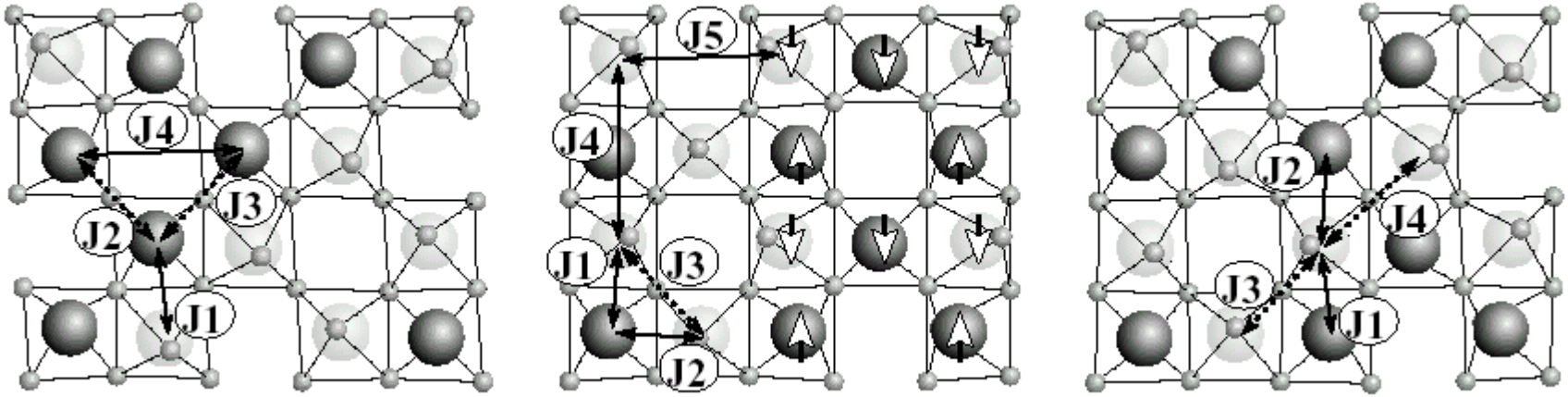

V atoms represented by large circles with different colors have different z-coordinate

Oxygen atoms are shown by small circles

Long range magnetic structure of CaV_3O_7 is depicted by white arrows

	CaV_2O_5	MgV_2O_5	CaV_3O_7	CaV_4O_9
$J1$	–28	60	46	62
$J2$	608	92	–14	89
$J3$	122	144	75	148
$J4$	20	19	18	91

QMC solution of Heisenberg model

Comparison of the calculated and measured susceptibility

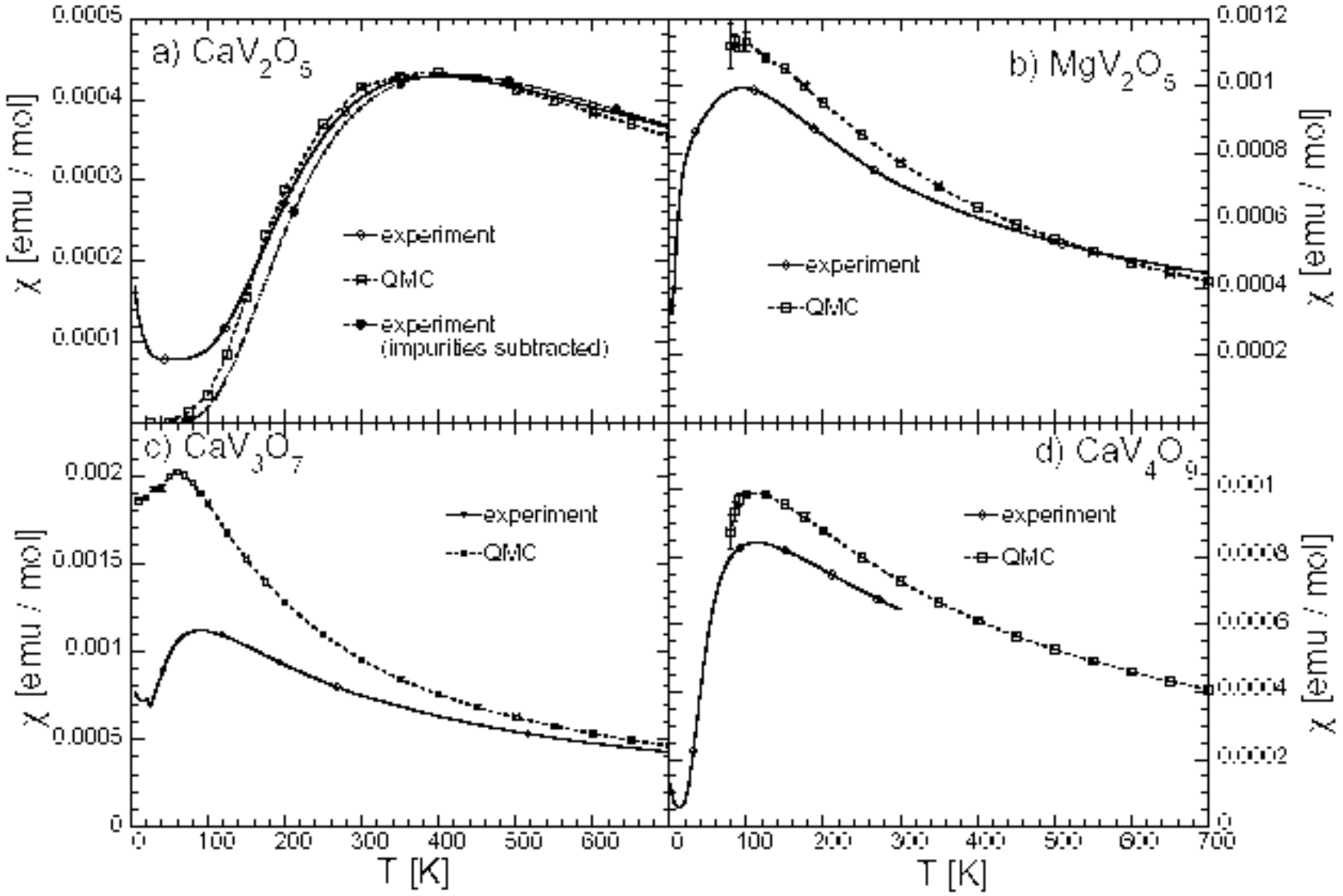

Orbital order in $KCuF_3$

$KCuF_3$ has cubic perovskite crystal structure

with Jahn-Teller distorted CuF_6 octahedra.

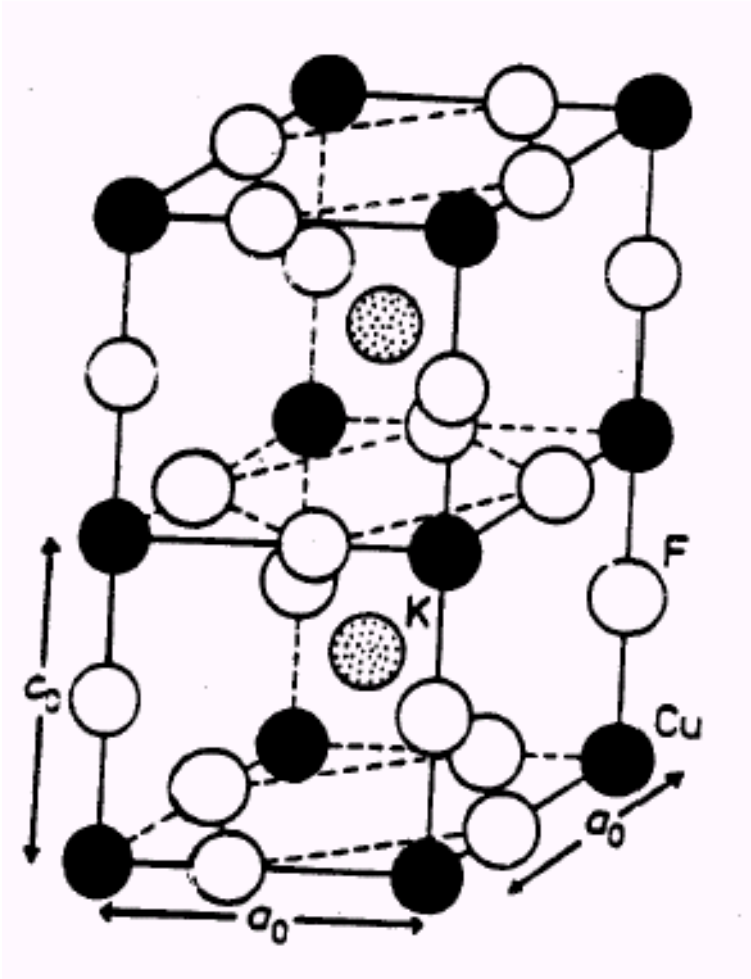

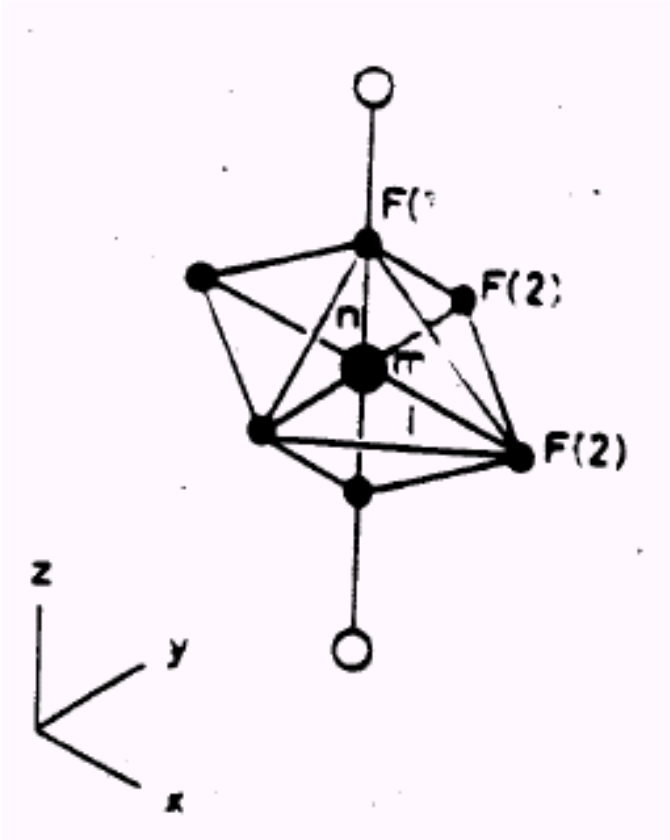

Orbital order in $KCuF_3$

In $KCuF_3$ Cu^{+2} ion has d^9 configuration **with a single hole in e_g doubly degenerate subshell.**

Experimental crystal structure

antiferro-orbital order

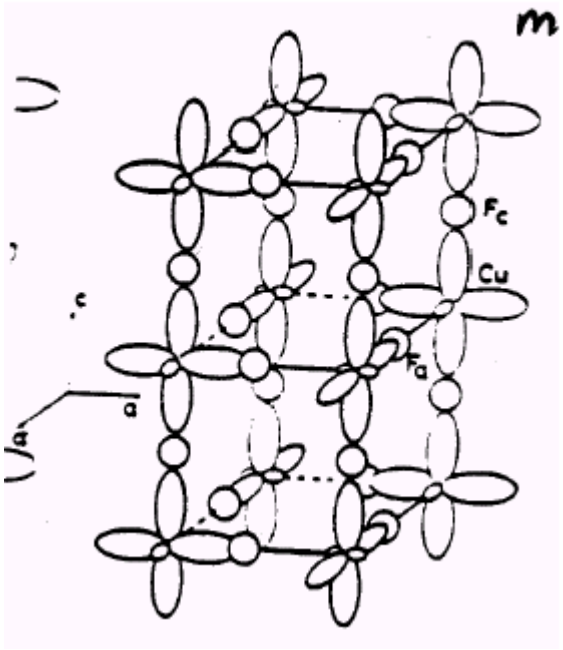

LDA+U calculations for *undistorted* perovskite structure

hole density of the same symmetry

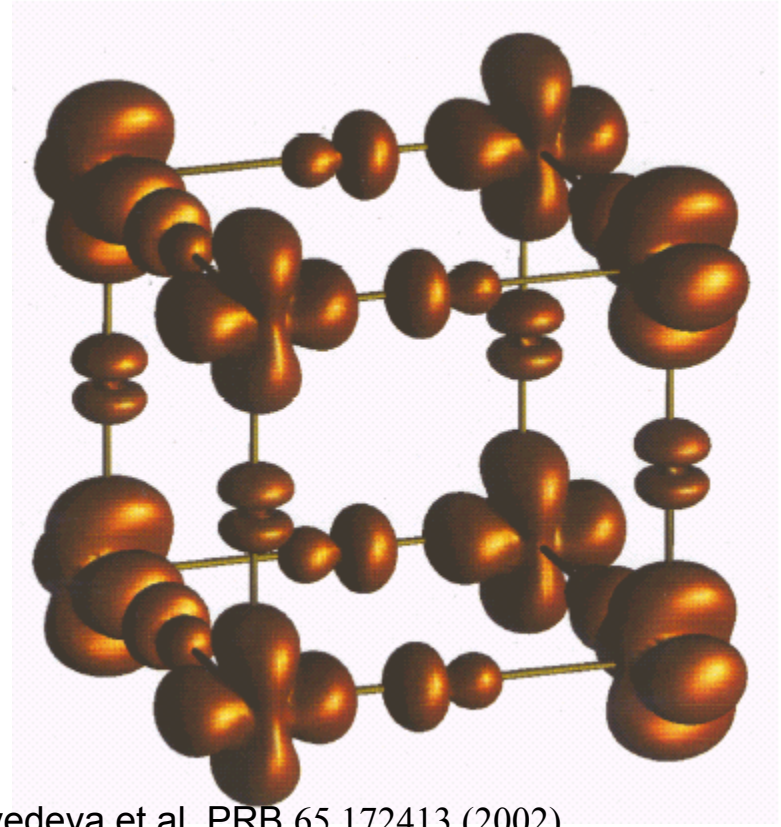

A.Lichtenstein et al, Phys. Rev.B **52,** R5467 (1995); J.Medvedeva et al, PRB 65,172413 (2002)

Cooperative Jahn-Teller distortions in $KCuF_3$

LSDA gave cubic perovskite crystal structure stable in respect to Jahn-Teller distortion of CuF_6 octahedra

Only LDA+U produces total energy minimum for distorted structure

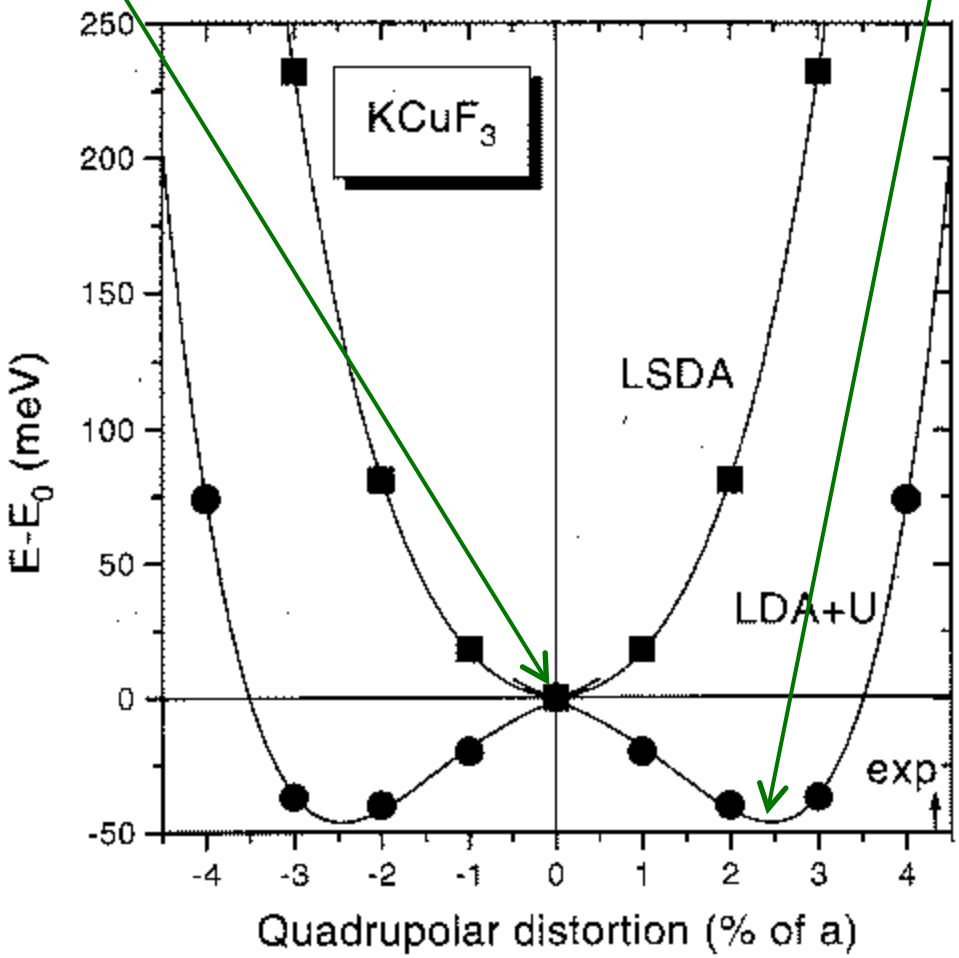

Calculated exchange couplings:
c-axis 17.5 meV
ab-plane –0.2 meV
One-dimensional antiferromagnet

Orbital order in $Pr_{1-x}Ca_xMnO_3$ (x=0 and 0.5)

$PrMnO_3$ has orthorhombic perovskite crystal structure

with tilted and rotated Jahn-Teller distorted MnO_6 octahedra.

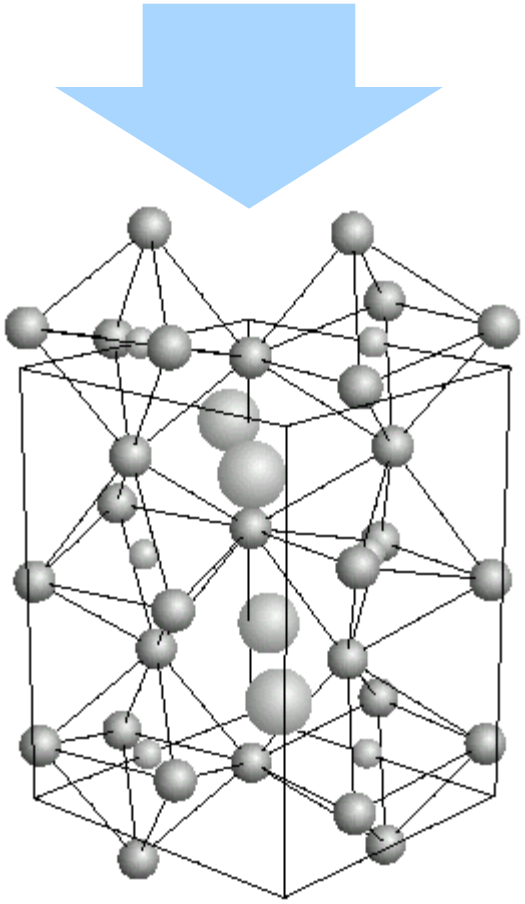

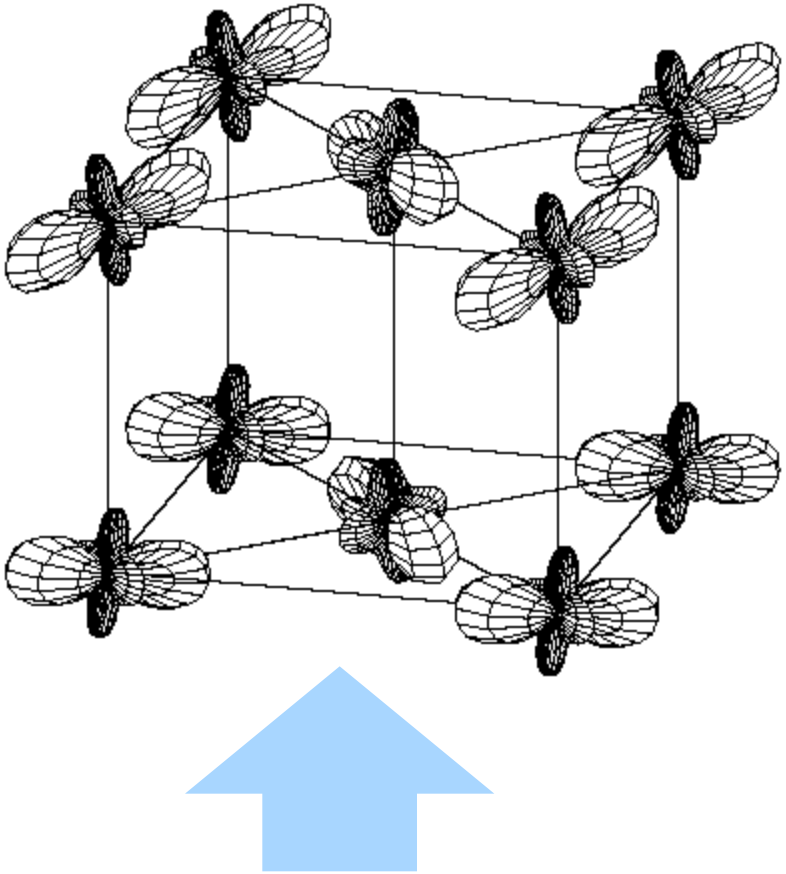

Orbital order for partially filled e_g shell of Mn^{+3} ion in $PrMnO_3$ in a crystal structure *without* JT-distortion from LDA+U

experimental magnetic and charge-orbital order

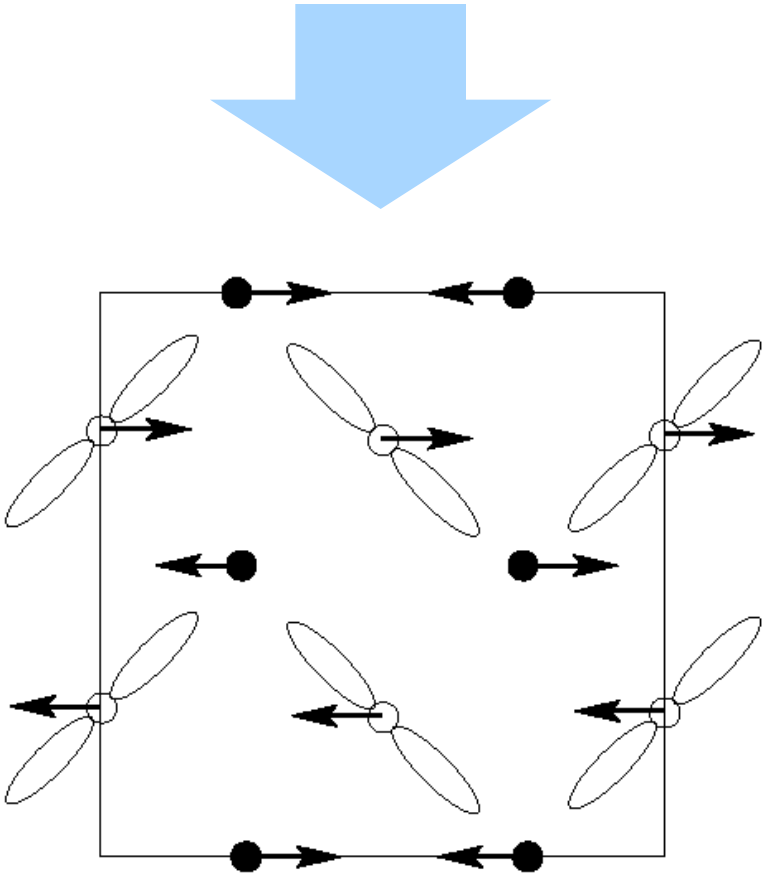

Orbital order for partially filled e_g shell of Mn^{+3} ion in $Pr_{0.5}Mn_{0.5}O_3$ in a crystal structure *without* JT-distortion from LDA+U

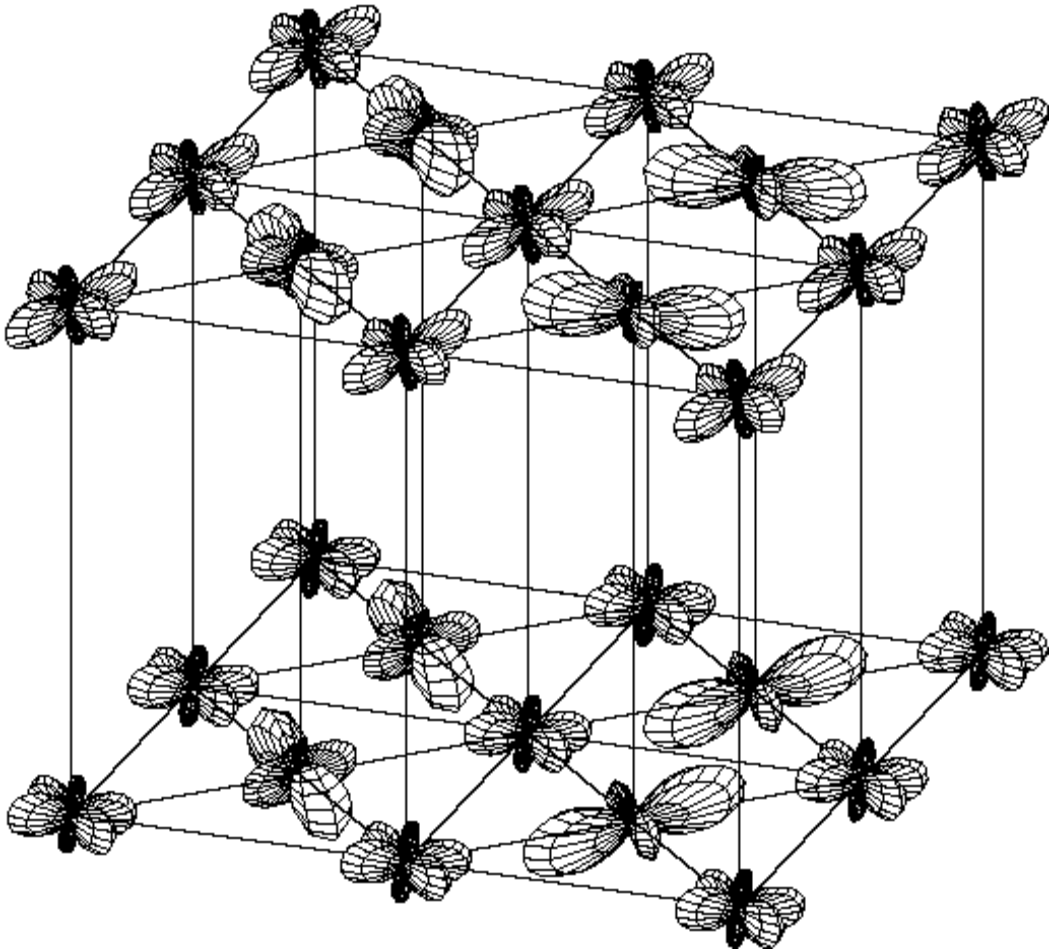

V.Anisimov et al, Phys.Rev.B **55**, 15 494 (1997); M.Korotin, PRB62, 5696 (2000)

Stripe formation in $Pr_{7/8}Sr_{1/8}MnO_3$

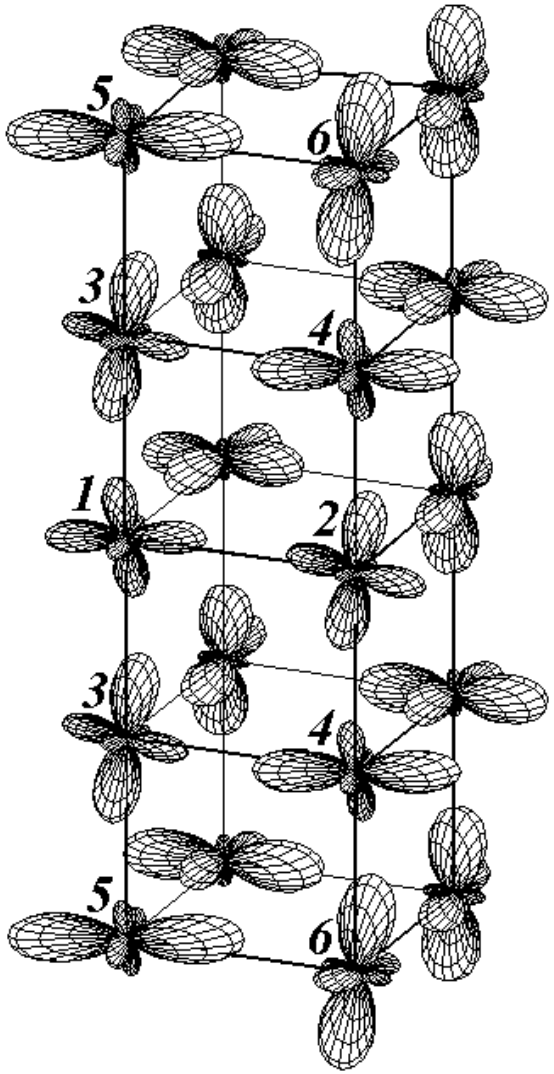

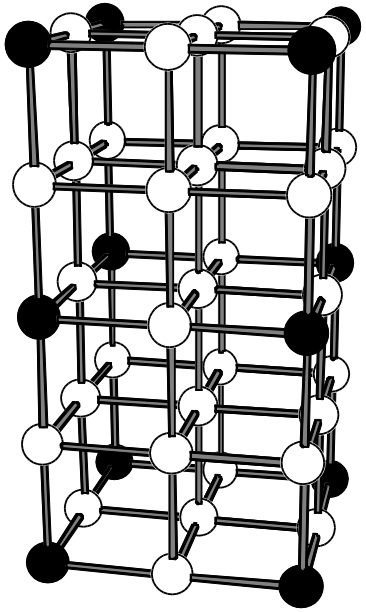

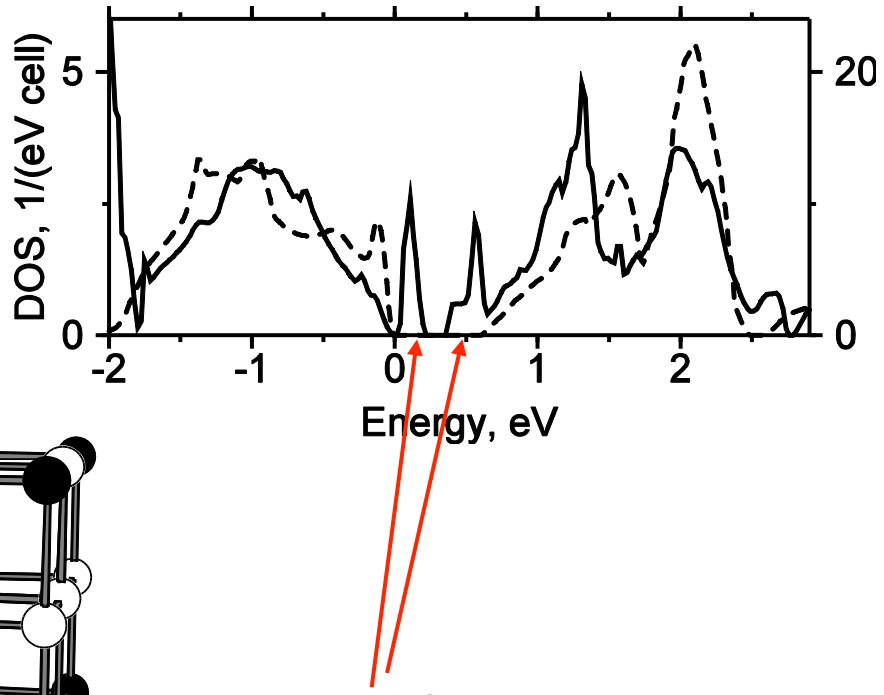

Polaron formation (solid line)
in Mott insulator (dashed line)

M.Korotin et al, PRB62, 5696 (2000)

Spin state of Co^{+3} in $LaCoO_3$

3d-level scheme for low-spin ground state

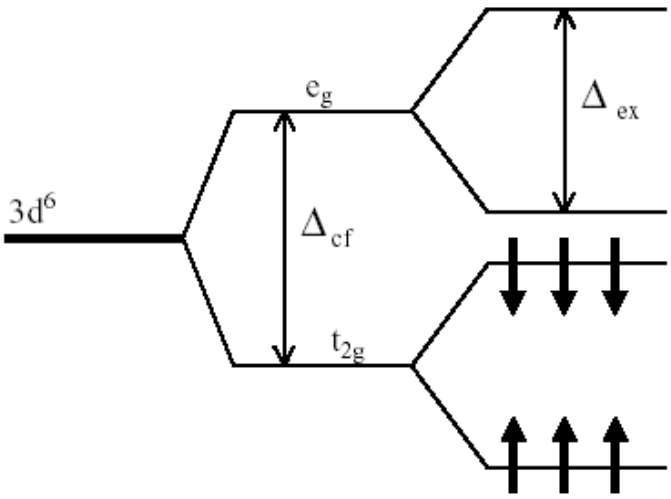

Scheme representation of various Co d^6+d^7L configurations in different spin states:

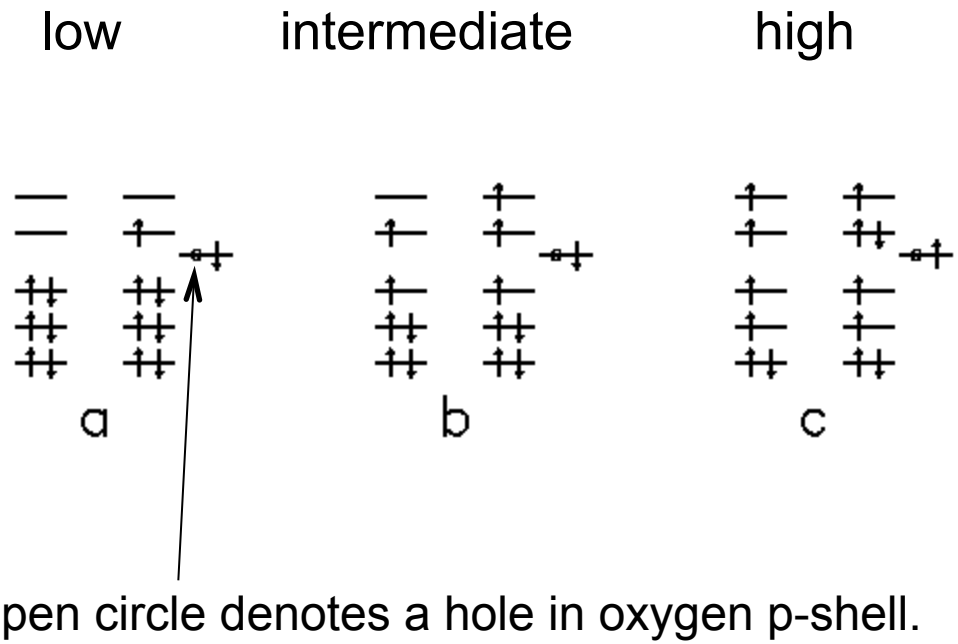

Open circle denotes a hole in oxygen p-shell.

M.Korotin et al, Phys.Rev.B **54** (1996) 5309

Spin state of Co^{+3} in $LaCoO_3$

The total energies for various spin states of $LaCoO_3$

relative to the energy of $t_{2g}^6 e_g^0$ state versus R3c lattice constant.

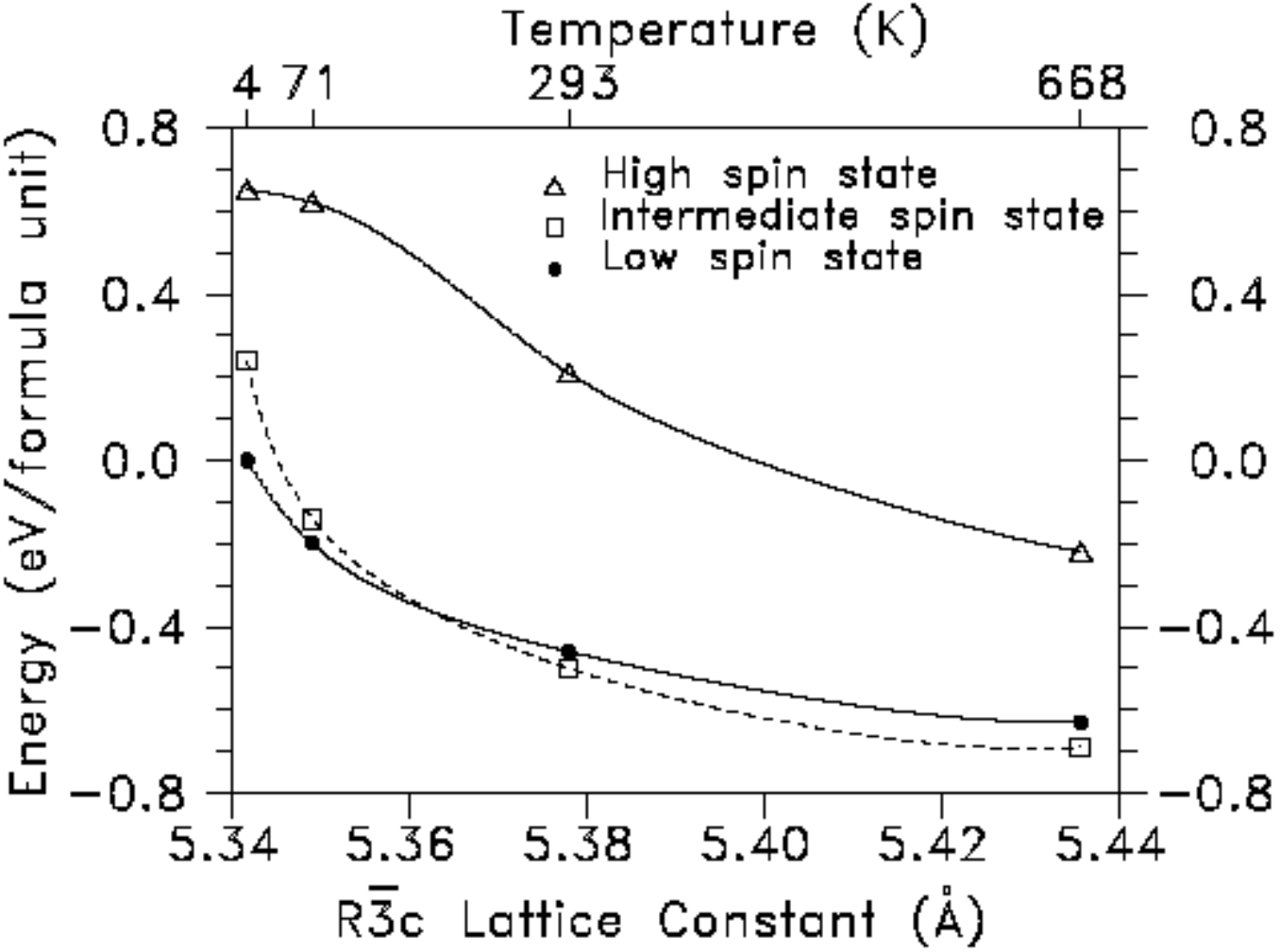

$HoCoO_3$ versus $LaCoO_3$

The rhombohedral crystal structure of $LaCoO_3$ (left) and the orthorhombic crystal structure of $HoCoO_3$ (right). Co - large spheres; O - small spheres.

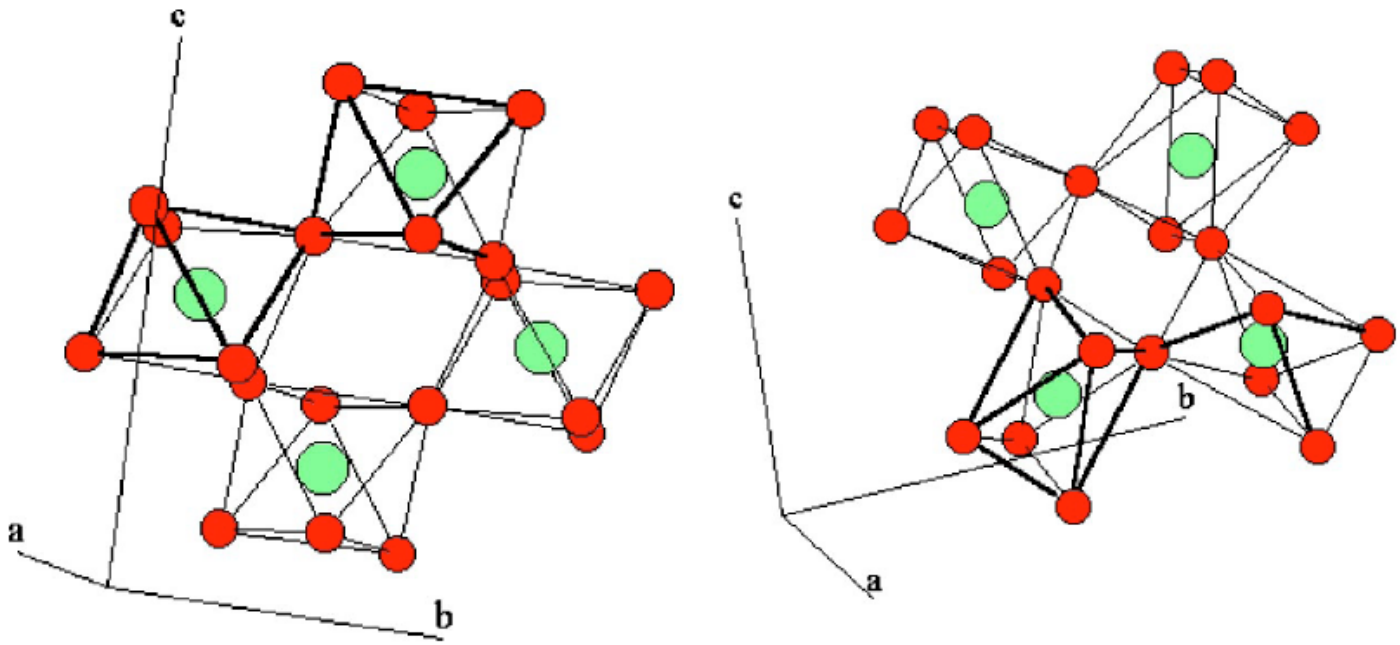

$HoCoO_3$ versus $LaCoO_3$

Comparison of total energy per Co ion of intermediate and low-spin state solutions for $LaCoO_3$ and $HoCoO_3$ calculated with the LDA+U approach as a functions of temperature. The temperature of transition is calculated as the temperature where two lines cross.

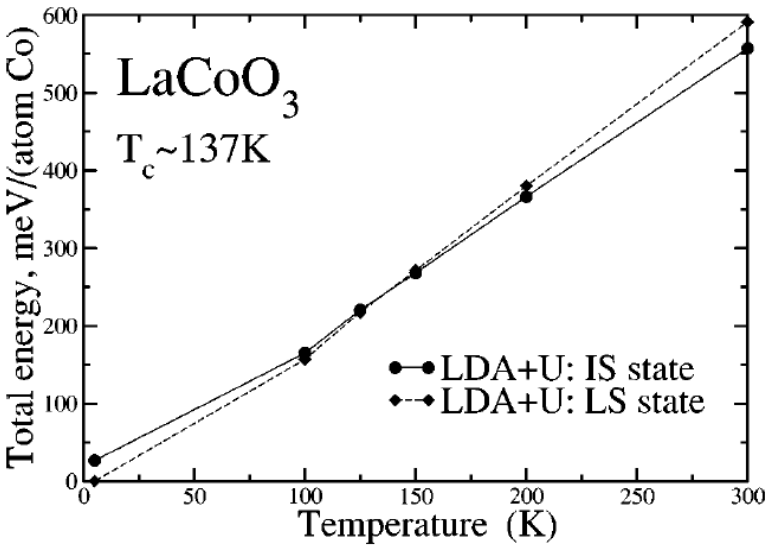

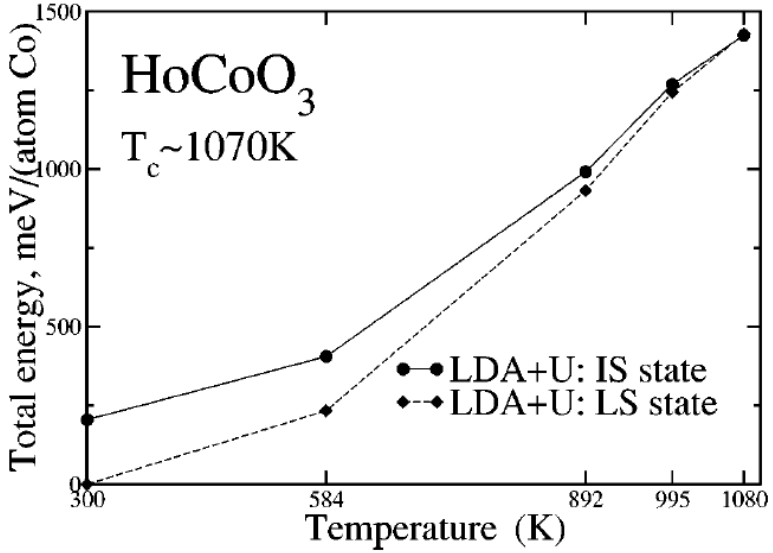

I. A. Nekrasov *et al*, PRB 68, 235113 (2003)

Magnetic transition in FeSi

Ground state of FeSi is a nonmagnetic semiconductor. With temperature increase material gradually becomes magnetic metal. LDA+U calculations show coexistence of two states.

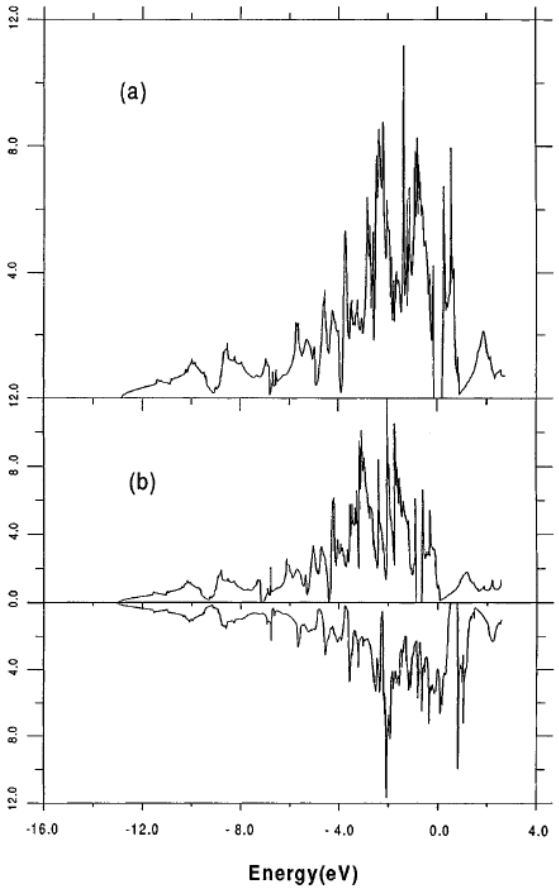

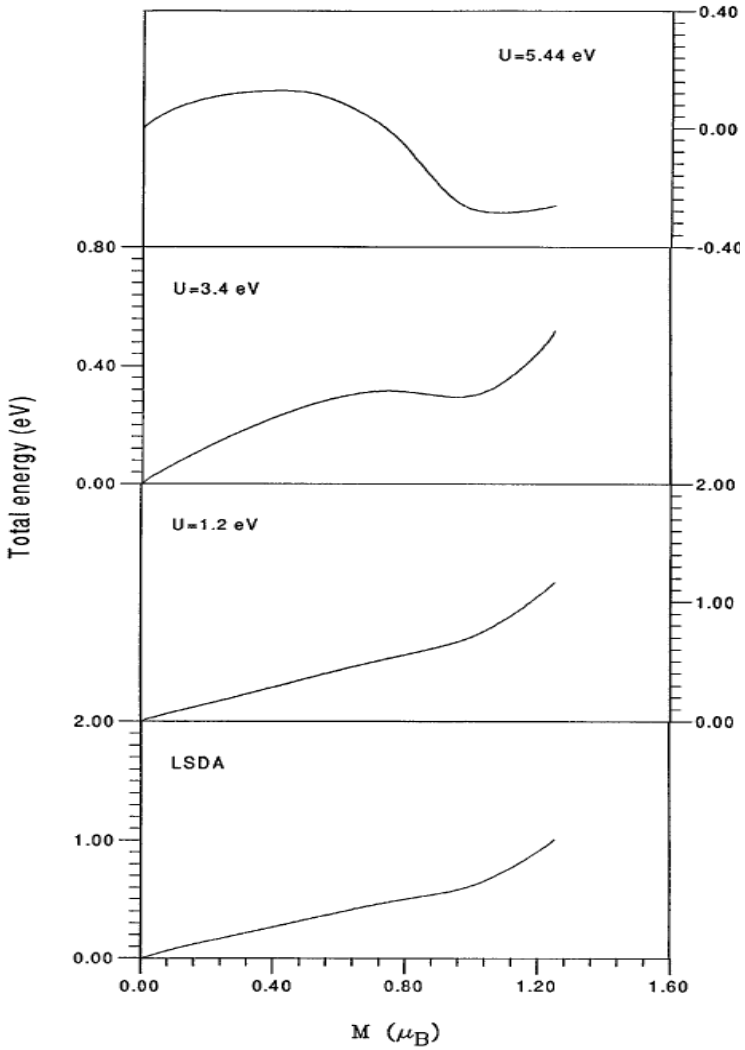

V.I.Anisimov *et al*, PRL 76, 1735 (1996)

Magnetic transition in $FeSi_{1-x}Ge_x$

Ground state of FeGe is a ferromagnetic metal. For alloy $FeSi_{1-x}Ge_x$ with increasing x transition to non-magnetic semiconductor is observed.

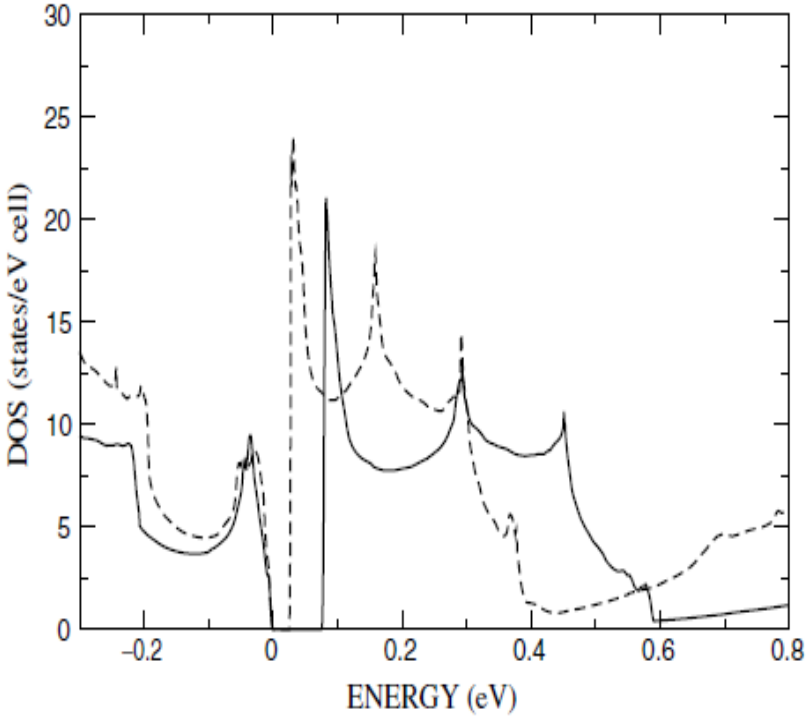

Density of states for FeSi (solid line) and for FeGe (dashed line)

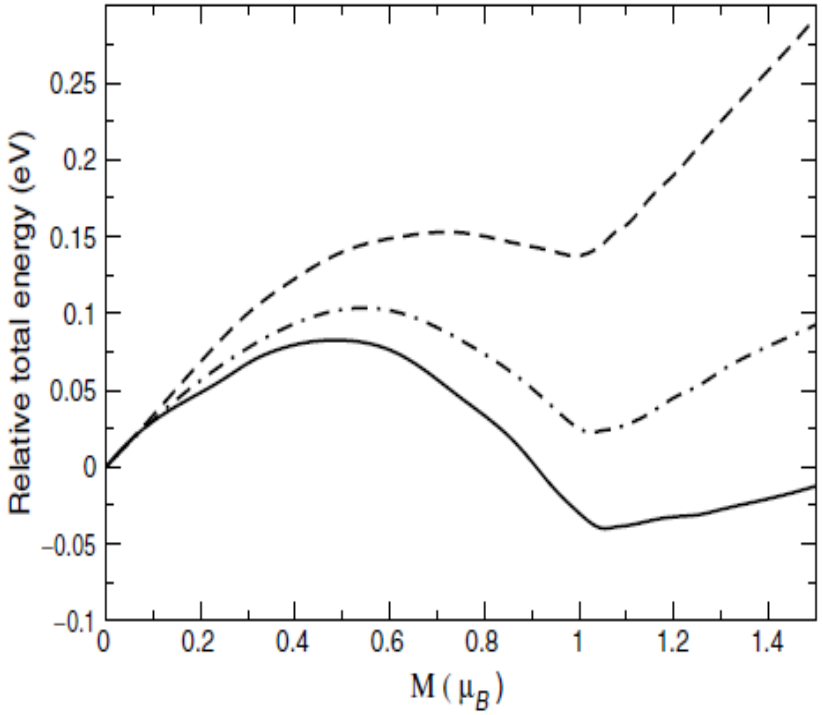

Total energy as a function of the spin moment M. The solid, dashed, and dash-dotted lines correspond to FeGe, FeSi, and $FeSi_{0:58}Ge_{0.42}$

V.I.Anisimov *et al*, PRL 89, 257203 (2002)

Magnetism due to vacancy states in TiO_{2-x}

Oxygen ion removal generates appearance of half-filled vacancy state in the energy gap that results in magnetic state

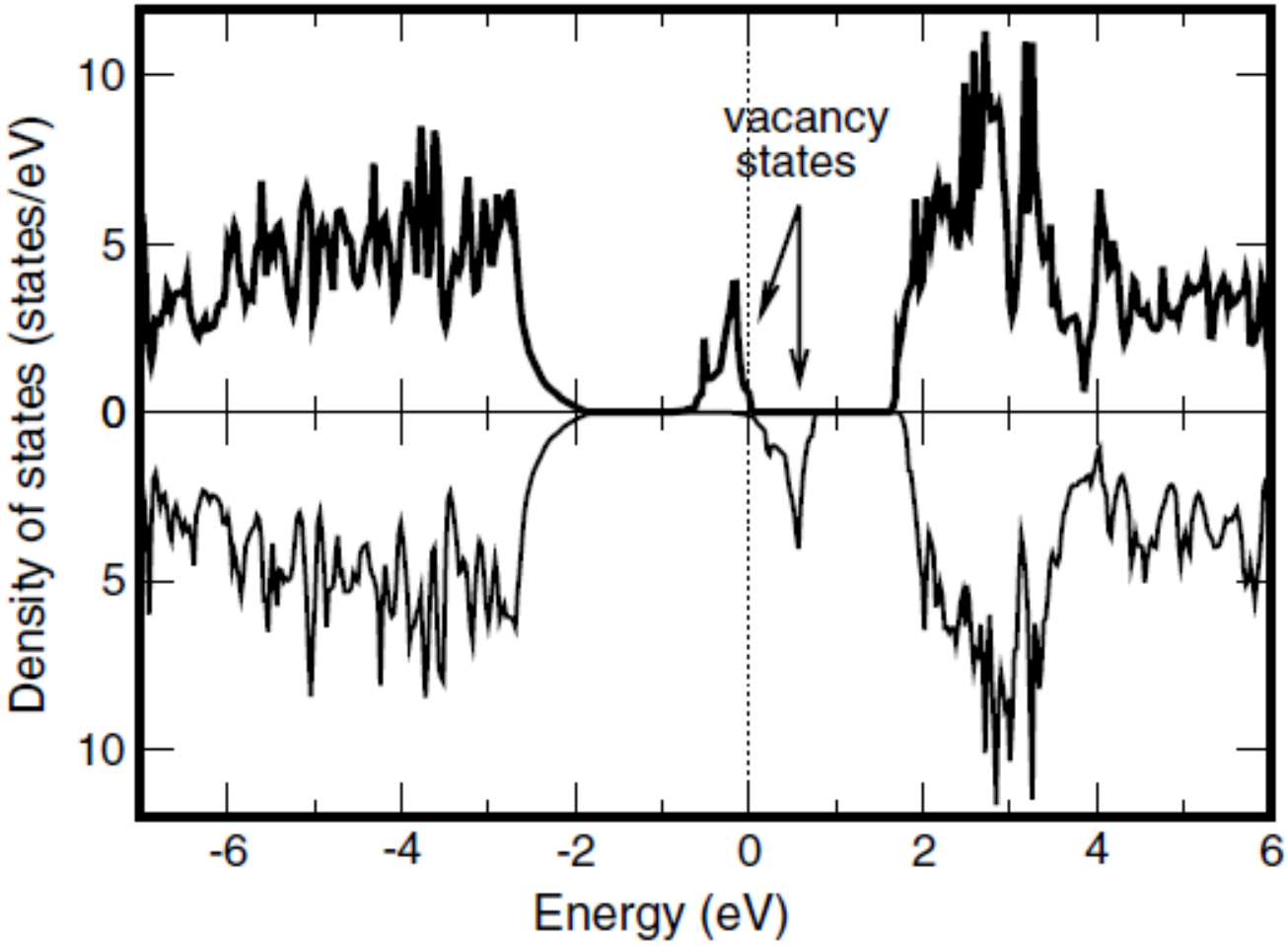

V.I.Anisimov *et al*, J. Phys.: Condens. Matter 18 (2006) 1695

Other LDA+U results

- **Exchange couplings in molecular magnet Mn-12 ($[Mn_{12}O_{12}(CH_3COO)_{16}(H_2O)_4]2CH_3COOH4H_2O$)**
  (PRB 65, 184435 (2002))
- **Insulating ground state of quarter-filled ladder NaV_2O_5 (PRB 66, 081104 (2002))**
- **CrO_2 : a self-doped double exchange ferromagnet**
  (PRL 80, 4305 (1998))
- **Mott-Hubbard insulator on Si-terminated SiC(0001) surface (PRB 61, 1752 (2000))**
- **Antiferromagnetism in linear-chain Ni compound $[Ni(C_6H_{14}N_2)_2]$ $[Ni(C_6H_{14}N_2)_2Cl_2]Cl_4$ (PRB 52,6975 (1995))**

LDA+U and LDA+DMFT

LDA+U
Static mean-field approximation
Energy-independent potential

$$\hat{V} = \sum_{mm'\sigma} | inlm\sigma > V^{\sigma}_{mm'} < inlm'\sigma |$$

LDA+DMFT
Dynamic mean-field approximation
Energy-dependent complex
self-energy operator

$$\hat{\Sigma}(\varepsilon) = \sum_{mm'\sigma} | inlm\sigma > \Sigma(\varepsilon)^{\sigma}_{mm'} < inlm'\sigma |$$

Applications:
Insulators with long-range
spin-,orbital- and charge order

Applications:
Paramagnetic, paraorbital
strongly correlated metals

Unsolved problem: short
range spin and orbital order

Dynamical cluster approximation (DCA)